INTERFACE

rsif.royalsocietypublishing.org

Research

Cite this article: Guo Y, Chang Z, Guo HY, Fang W, Li QY, Zhao HP, Feng XQ, Gao H. 2018 Synergistic adhesion mechanisms of spider capture silk. *J. R. Soc. Interface* **15**: 20170894.
http://dx.doi.org/10.1098/rsif.2017.0894

Received: 30 November 2017
Accepted: 12 February 2018

Subject Category:
Life Sciences–Physics interface

Subject Areas:
biomimetics

Keywords:
spider silk, adhesion, synergistic mechanism, energy absorption, strength, biomechanics

Authors for correspondence:
Xi-Qiao Feng
e-mail: fengxq@tsinghua.edu.cn
Huajian Gao
e-mail: huajian_gao@brown.edu

†These authors contributed equally to the study.

Electronic supplementary material is available online at https://dx.doi.org/10.6084/m9.figshare.c.4010344.

THE ROYAL SOCIETY PUBLISHING

Synergistic adhesion mechanisms of spider capture silk

Yang Guo[1,†], Zheng Chang[3,†], Hao-Yuan Guo[1], Wei Fang[1], Qunyang Li[1,2], Hong-Ping Zhao[1], Xi-Qiao Feng[1,2] and Huajian Gao[4]

[1]AML, Department of Engineering Mechanics, and [2]State Key Laboratory of Tribology, Tsinghua University, Beijing 100084, People's Republic of China
[3]College of Science, China Agricultural University, Beijing 100083, People's Republic of China
[4]School of Engineering, Brown University, Providence, RI 02912, USA

XQF, 0000-0001-6894-7979

It is well known that capture silk, the main sticky component of the orb web of a spider, plays an important role in the spider's ability to capture prey via adhesion. However, the detailed mechanism with which the spider achieves its unparalleled high-adhesion performance remains elusive. In this work, we combine experiments and theoretical analysis to investigate the adhesion mechanisms of spider silk. In addition to the widely recognized adhesion effect of the sticky glue, we reveal a synergistic enhancement mechanism due to the elasticity of silk fibres. A balance between silk stiffness, strength and glue stickiness is crucial to endow the silk with superior adhesion, as well as outstanding energy absorption capacity and structural robustness. The revealed mechanisms deepen our understanding of the working principles of spider silk and suggest guidelines for biomimetic designs of spider-inspired adhesion and capture devices.

1. Introduction

Surface adhesion is critical for many important applications in mechanical and biomedical engineering [1], micro-electromechanical systems [2], robotics [3], as well as in our daily life [4]. Biological materials and tissues with special adhesion properties, e.g. gecko toes [5], frog tongues [6] and marine mussels [7], have aroused the curiosity of scientists and engineers. Much effort has been directed towards understanding the physical mechanisms of adhesion of biological materials [8,9]. Spider capture silk is a prominent example of using adhesion to intercept and subdue prey that are much larger than a spider's size [10]. Spiral orb webs are used by more than 3000 species of spiders for prey capture (figure 1*a*) [12]. As the main sticky component in a spider orb-web, the capture silk is capable of catching a wide range of prey including insects (e.g. bees, flies and locusts) and even small animals (e.g. birds and bats) [13–17]. A capture silk thread comprises two twisted strands [18], with an elastic modulus about 10 times lower than that of the radial silk [19,20]. In contrast to the smooth and non-sticky radial silk thread, the capture silk thread is coated with a layer of sticky glue [21]. As a consequence of Rayleigh instability [22], the coating glue typically breaks into uniformly distributed droplets, rendering a unique bead–chain appearance (figure 1*b*). Each glue droplet is composed of a glycoprotein core surrounded by a viscous aqueous coating [18] and can be stretched substantially to accommodate a large strain [23]. The glycoprotein core works as an anchor which fixes the glue droplet to the axial fibres of the capture thread and transfers the load from the capture thread to the droplets [24]. During a prey capture process, the deformed glue droplets, together with the silk thread, form a structure like a suspension bridge [22,25,26]. The suspension bridge structure [23,26,27] plays a vital role in capturing prey items, which recruits the adhesion of glue droplets [26], enhances the stickiness of capture silk and dissipates the kinetic energy of prey items via the deformation of capture thread and glue droplets [23].

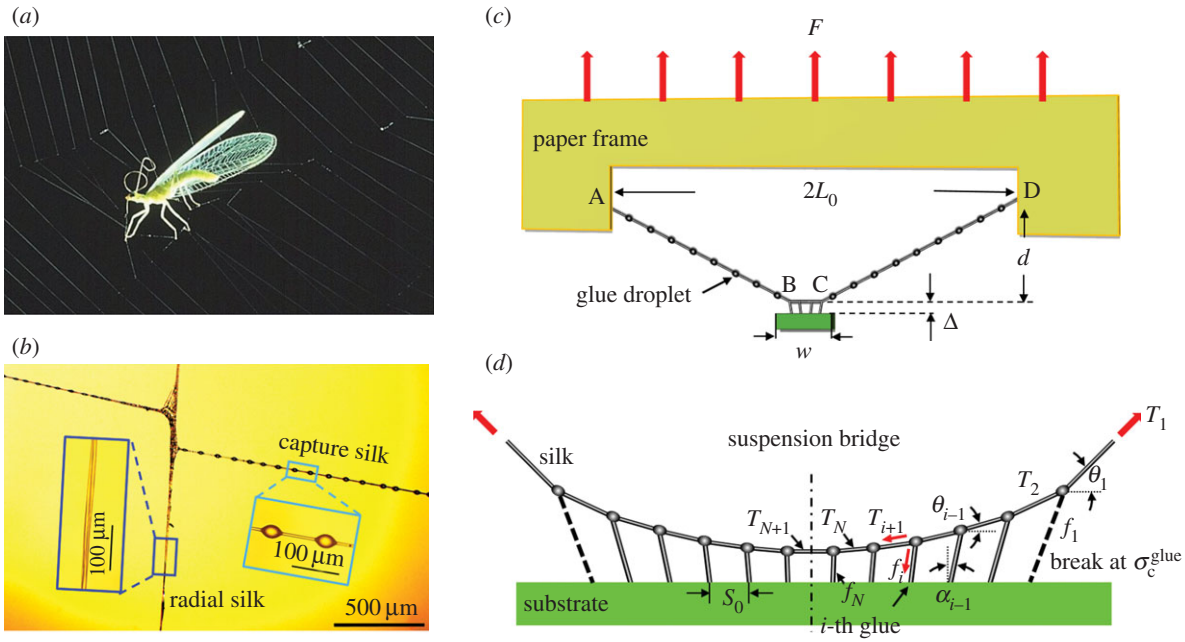

Figure 1. Experiment and theoretical model for peeling an adhered spider capture silk thread from a rigid substrate. (*a*) An insect is subdued by capture silk fibres of a spider web [11]. (*b*) A magnified view of the local morphology of a web. The insets show the smooth morphology of a radial silk thread and the bead–chain structure of the capture silk–thread. (*c*) A schematic showing the peeling experiment of a capture silk thread adhered on a substrate and (*d*) the theoretical model of the silk–substrate system. Δ in (*c*) denotes the extension of glue droplets. (Online version in colour.)

The mechanical properties of glue droplets have a great influence on the suspension bridge structure [25,28]. Previous studies have found that the mechanical properties of glue droplets are largely dependent on the contact state and ambient conditions, e.g. humidity [29–32], temperature [33] and UV radiation [34]. Better spreading of the glue on a substrate surface enhances adhesion [35] and higher humidity is propitious to enlarge the ultimate extensibility of glue droplets [30]. Furthermore, variations in nutrition intake of the spider [36] and salt content in viscid glue droplets [37] also influence the adhesion performance of glue droplets.

So far, the remarkable adhesion capability of capture silk threads has been primarily attributed to the strong stickiness of the glue droplets. However, a recent study has shown that the stickiness of silk glue seems to correlate with the strength of capture silk fibre [27]. Open questions include how the elasticity and strength of capture silk fibre affect its adhesion capability and whether there exists an optimal relation between the properties of silk fibre and glue droplets.

In this work, to better understand the physical mechanisms underlying the adhesive characteristics of spider capture silk, we conducted peeling experiments to measure the peeling behaviour of a capture silk bonded to a substrate. Based on the experimental results, a theoretical model was developed to quantitatively describe the slow and quasi-static detachment process. Our analysis suggests that the stiffness and strength of the capture silk thread play equally important roles as the stickiness of the glue in controlling the adhesion performance of the silk. A synergistic optimization of these properties endows the silk with its outstanding energy absorption capacity in capturing prey while maintaining structural integrity.

2. Material and methods

Adult spiders *Araneus ventricosus*, with an average body size of approximately 2 cm, were raised in our laboratory. Once a web was produced, a portion of the fresh capture silk thread (with an initial length of $2L_0 = 2.8$ cm) was transferred and fixed to a bow-shaped cardboard for testing within 24 h. The capture silk thread had a typical diameter of 6.2 µm and a cross-sectional area of $A_0 = 30.2\ \mu m^2$ and the glue droplets on the silk thread were ellipsoidal in shape [38], with major and minor axes of about 50 µm and 30 µm, respectively. The average spacing between neighbouring glue droplets s_0 was found to be around 112.5 µm.

To quantify the adhesion properties of the capture silk, we peeled the silk thread from a solid substrate, mimicking the escape process of a prey, while measuring the peeling force and recording the deformation of the silk thread and glue droplets. The substrate was made of polydimethylsiloxane (PDMS) block with an elastic modulus of approximately 1 MPa and had a width of $w = 2.7$ mm and a thickness of 2 mm. Here we chose PDMS as the substrate material for two reasons. First, the strong interfacial strength between PDMS and the glue droplets can retard their debonding. Second, the PDMS blocks of different sizes can be easily fabricated and fixed in the testing machine we used. During the peeling test, the PDMS substrate was fixed to the lower grip of a testing machine and the cardboard fixture was pulled at a constant speed of $0.1\ mm\ s^{-1}$ (figure 1*c*; electronic supplementary material). The force was measured by a nanomechanical tensile testing machine (Agilent T150 UTM), while the deformation was recorded by a high-speed camera (Fastcam Mini UX100, Photron, Japan) with a microscope lens (QM100, Questar). In addition to the peeling tests, independent uniaxial tension tests were performed using the same tensile testing machine to measure the elastic modulus E_s (electronic supplementary material) and the rupture strain ε_c^{silk} of the capture silk. All experiments were conducted under ambient conditions, with temperature maintained at around 24°C and the relative humidity at 60–70%. The potential variability of mechanical properties induced by the environmental factors [29–35] was expected to be small in our tests and will not be discussed further.

We here develop a theoretical model to analyse the suspension bridge mechanism [23,26,27] in the detachment process

when the silk thread with sticky glue droplets is pulled from a rigid substrate, as shown in figure 1. As the deformation of the PDMS block is negligible compared to the deformation of the glue droplets and the capture silk thread (for more discussions, see electronic supplementary material), the rigid substrate assumption is a reasonable approximation. The glue droplets and the silk fibre are assumed to be linear elastic upon stretch [39], and the corresponding spring constant of an individual glue droplet during stretch is K_g (electronic supplementary material) and silk fibre is $K_s = E_s A_0/L$ for a given length L, respectively. When the two ends of the silk thread are pulled by a relative displacement d (distance between the glue droplet and the contact zone; figure 1*c*), the tensile strain in the suspended segment of the silk thread (parts AB and CD in figure 1*c*) is $\varepsilon = (1 - \cos\theta_1)/\cos\theta_1$, where $\theta_1 = \arctan[2d/(2L_0 - w)]$ is the tilt angle of the suspended segment due to vertical loading force F. The corresponding tension in the suspended silk thread is

$$T_1 = E_s A_0 \frac{1 - \cos\theta_1}{\cos\theta_1}. \tag{2.1}$$

The external force F exerted on the system is related to T_1 as

$$F = 2T_1 \sin\theta_1. \tag{2.2}$$

For a quasi-static loading, the total energy absorbed by the silk thread and glue droplets equals to the work done by the external force to remove an adhered item from the silk–glue system, i.e. $U_t = \int_0^{d+\Delta} F(\delta)\,\mathrm{d}\delta$, where $F = F(\delta)$ is a function of the total displacement δ.

The mechanical and geometrical properties of the silk–substrate system in the contact zone during peeling are described by parameters T_i, θ_i, f_i and α_i, as shown in figure 1*d* (electronic supplementary material); T_i denotes the tensile force in the i-th segment of the silk, and its tilt angle θ_i is measured from the horizontal direction; f_i is the tensile force in the i-th elongated glue droplet, and its incline angle α_i is measured from the vertical direction. Under a specified external force F, the above parameters can be determined from geometric relations and force equilibrium conditions. The forces acting on each glue droplet satisfy the equilibrium equations along the horizontal direction:

$$T_{i+1}\cos\theta_{i+1} - T_i\cos\theta_i + \bar{f}_i = 0, \tag{2.3}$$

where $\bar{f}_i = f_i \sin\alpha_i$ and i takes the value from 1 to N. When $i = N$, the $(N+1)$-th silk segment is the horizontal part of the silk thread in the middle and $\theta_{N+1} = 0$. Along the vertical direction, the equilibrium equations are

$$T_{i+1}\sin\theta_{i+1} - T_i\sin\theta_i + \tilde{f}_i = 0, \tag{2.4}$$

where $\tilde{f}_i = f_i \cos\alpha_i$ and i takes the value from 1 to N. Equations (2.3) and (2.4) result in $2N$ constraints for N glue droplets in the half contact zone. For the deformed glue droplets and silk segments from 1 to $N-1$, the geometric compatibility of angular relations requires

$$\frac{\tilde{f}_i - \tilde{f}_{i+1}}{\bar{f}_i - \bar{f}_{i+1} + K_g s_0} = \tan\theta_{i+1}, \tag{2.5}$$

resulting in $N-1$ equations. The geometric compatibility of glue droplet lengths

$$\left(\frac{\bar{f}_i}{K_g} + s_0 - \frac{\bar{f}_{i+1}}{K_g}\right)^2 + \left(\frac{\tilde{f}_i}{K_g} - \frac{\tilde{f}_{i+1}}{K_g}\right)^2 = s_0^2\left(\frac{T_{i+1}}{E_s A_0} + 1\right)^2, \tag{2.6}$$

also lead to $N-1$ equations. When $i = N$, equation (2.6) becomes

$$\frac{\bar{f}_N}{K_g} = \frac{s_0}{2}\frac{T_{N+1}}{E_s A_0}. \tag{2.7}$$

Thus, the $4N+1$ unknown parameters T_{i+1}, θ_i, f_i and α_i in the silk–prey system can be determined from the $4N+1$ equations in equations (2.1)–(2.7) for any given F. A trust-region algorithm was employed to solve these nonlinear and coupled equations.

During the peeling process, the adhesion of the silk–glue system may fail in two different ways, i.e. by breaking the capture silk thread or by breaking the glue–substrate adhesion. Our experiments show that for the former rupture mode, the silk fibres break when their tensile strain exceeds a threshold ε_c^{silk}. For the latter, the elongated glue droplets are detached from the substrate when their tensile force F^{glue} reaches a critical value F_c^{glue}, corresponding to an adhesive strength of $\sigma_c^{glue} = F_c^{glue}/A_g$, A_g being the adhesion area at detachment, between the glue and substrate. In our model, we estimate the spring constant of the glue droplet to be $K_g = 0.31\ \mathrm{N\,m^{-1}}$ and the adhesive strength $\sigma_c^{glue} = 0.245$ MPa. Independent uniaxial tensile tests give the critical fracture strain of the capture silk as $\varepsilon_c^{silk} = 0.8$.

3. Results and discussions

3.1. Peeling of a capture silk thread from a substrate

In the peeling experiments, deformation states of the silk thread and stretched glue droplets can be clearly observed. Three typical snapshots of a peeling test are shown in figure 2*a* and the whole process is recorded as electronic supplementary material, video S1. The corresponding theoretical results at different moments are given in figure 2*b*. Comparison of figure 2*a*,*b* indicates that the theoretical model can reasonably capture the essential features of deformation and failure in the process. As shown by the experimental and theoretical force–displacement curves in figure 2*c*, the peeling process can be divided into three typical stages via the suspension bridge mechanism: pre-debonding (I), stable-debonding plateau (II) and unstable detachment (III). It is noted that the area below the force–displacement curve, U_t, represents the energy absorption capacity of the capture silk during peeling and the energy barrier that prevents a prey from escaping.

During the first stage of peeling, both the silk fibre and the glue droplets are stretched and the glue–substrate interface remains intact as the silk thread is loaded. This stage can be further divided into two sub-regimes. Initially, when the displacement d is relatively small, the force increases slowly with increasing displacement and the load is primarily carried by a small number of glue droplets around the edge of the contact zone. In the later part of stage I, the force increases more rapidly with increasing displacement because more and more glue droplets are stretched. The gradual involvement of the glue droplets results in the nonlinear feature of the force–displacement curve.

At stage II (time t_2 in figure 2*a*), the glue droplets at the edge of the contact zone reach their ultimate adhesion strength and begin to detach from the substrate. However, as the middle glue droplets are still getting strengthened, the total force in the silk thread remains fairly constant (figure 2*c*) but with local fluctuations. The silk–substrate system evolves stably as the glue droplets sequentially break near the edge (see electronic supplementary material, video S1). Because of the unique bead–chain structure of capture silk thread, the silk–substrate system has a persistent energy absorption capability in stage II. In this way, attachment of a certain number of droplets can efficiently prevent the escape of energetic prey.

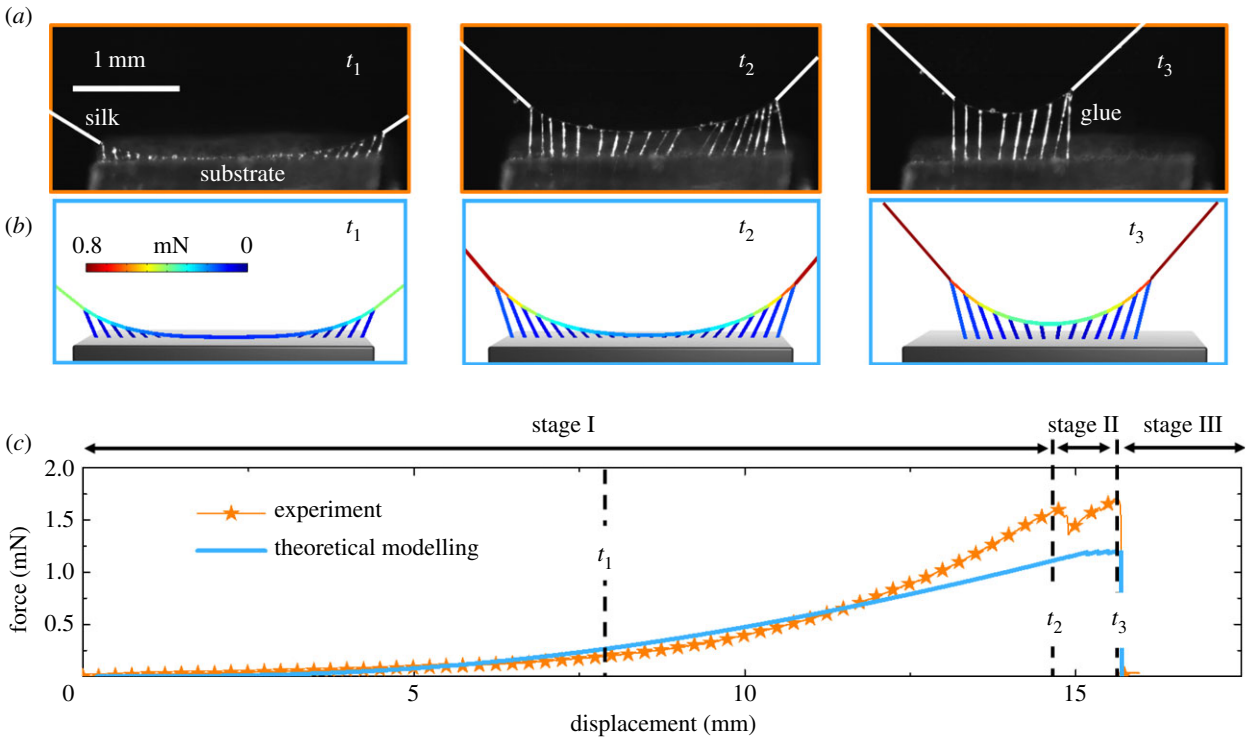

Figure 2. Experiments and theoretical modelling of a capture silk thread detached from a PDMS substrate. (*a*) Three typical snapshots at time t_1, t_2 and t_3 in the peeling experiment, and (*b*) the corresponding theoretical predictions. The colours in the structure indicate the magnitude of the force in the silk thread and glue droplets. (*c*) Experimental and theoretical force–displacement curves during the peeling process. (Online version in colour.)

As the external displacement keeps increasing, the system reaches a critical point ($d_{max} \sim 15.7$ mm in the test) and the remaining glue droplets start to break simultaneously leading to a final detachment of the silk thread, depicted as stage III in figure 2. In all peeling tests, we do not observe failure of the silk fibre. Rupture occur at the glue–substrate interfaces and the silk fibres remain intact after the peeling test [27]. There seems to be a self-protection mechanism that helps protect the structural integrity of the orb webs from accidental damage [27]. This means that overly strong prey would be allowed to escape and the web can survive and rejuvenate after the glue droplets are regenerated.

The above experiments and analysis suggest that the capture silk may have evolved different strategies in capturing prey with different sizes and weights. When weaker prey is adhered, the capture silk mainly utilizes the elasticity of its fibre, and the glue droplets only undergo small deformation. For larger prey, more glue droplets participate in the capturing process to provide a larger force. When the prey is too strong to be captured, the glue droplets will get detached prior to failure of the silk thread, thereby minimizing the damage to the web (stages II and III).

In our model, the glue droplets are fixed to the axial fibres of the capture thread and no relative sliding along the axial fibres is allowed. However, sliding between some glue droplets and capture silk fibre could also occur in our experiments. This seems to be another self-protection mechanism. When the shear force on one glue droplet reaches the interfacial strength between the glycoprotein core and the droplet, it will slide along the silk and lower the stress in it. This mechanism can homogenize the forces on the droplets to make full use of the middle glue droplets [26] and reduce the possibility of rupture of single glue droplet.

As can be seen from figure 2*b*, the force–displacement curve in the peeling process predicted by the theoretical model agrees reasonably well with the experimental measurement. Because the theoretical model can provide detailed information about the structure, we use it to explore possible optimization strategies of the capture silk.

3.2 Synergistic effect between silk stiffness, strength and glue stickiness

As demonstrated by the above experiments and analysis, both silk deformation and glue droplet adhesion affect the detachment behaviour of a capture silk thread peeled from a substrate. In this section, we quantitatively examine how the stiffness of the capture silk thread, characterized by its elastic modulus E_s and the stickiness of the glue droplets, characterized by its adhesive strength σ_c^{glue}, influence the peeling process. With that goal in mind, we systematically vary both E_s and σ_c^{glue} and calculate the force–displacement detachment curve for each combination using our theoretical model. In the simulations, six combinations are tested: E_s is chosen to be 2.5 MPa, 50 MPa or 1 GPa; and σ_c^{glue} takes the value of 0.12 MPa or 0.245 MPa. It is noted that the combination of $E_s = 50$ MPa and $\sigma_c^{glue} = 0.245$MPa corresponds to the actual mechanical properties of the real capture silk used in our experiments. It is noted that the elastic modulus $E_s = 50$ MPa of the capture silk thread is larger than the commonly reported values [40,41] due to the equivalent linearization of the elastic behaviour (more detailed discussions are given in electronic supplementary material). The mechanical parameters of the capture thread used in our analysis are taken on the basis of our experiments and slightly different from those given by Elettro *et al*. [39]. All other parameters, e.g. the silk length L_0, the silk cross-sectional area A_0, the critical fracture strain of the capture silk ε_c^{silk}, spring constant of the glue droplet K_g, ultimate adhesion area of the glue droplet A_g and the contact zone

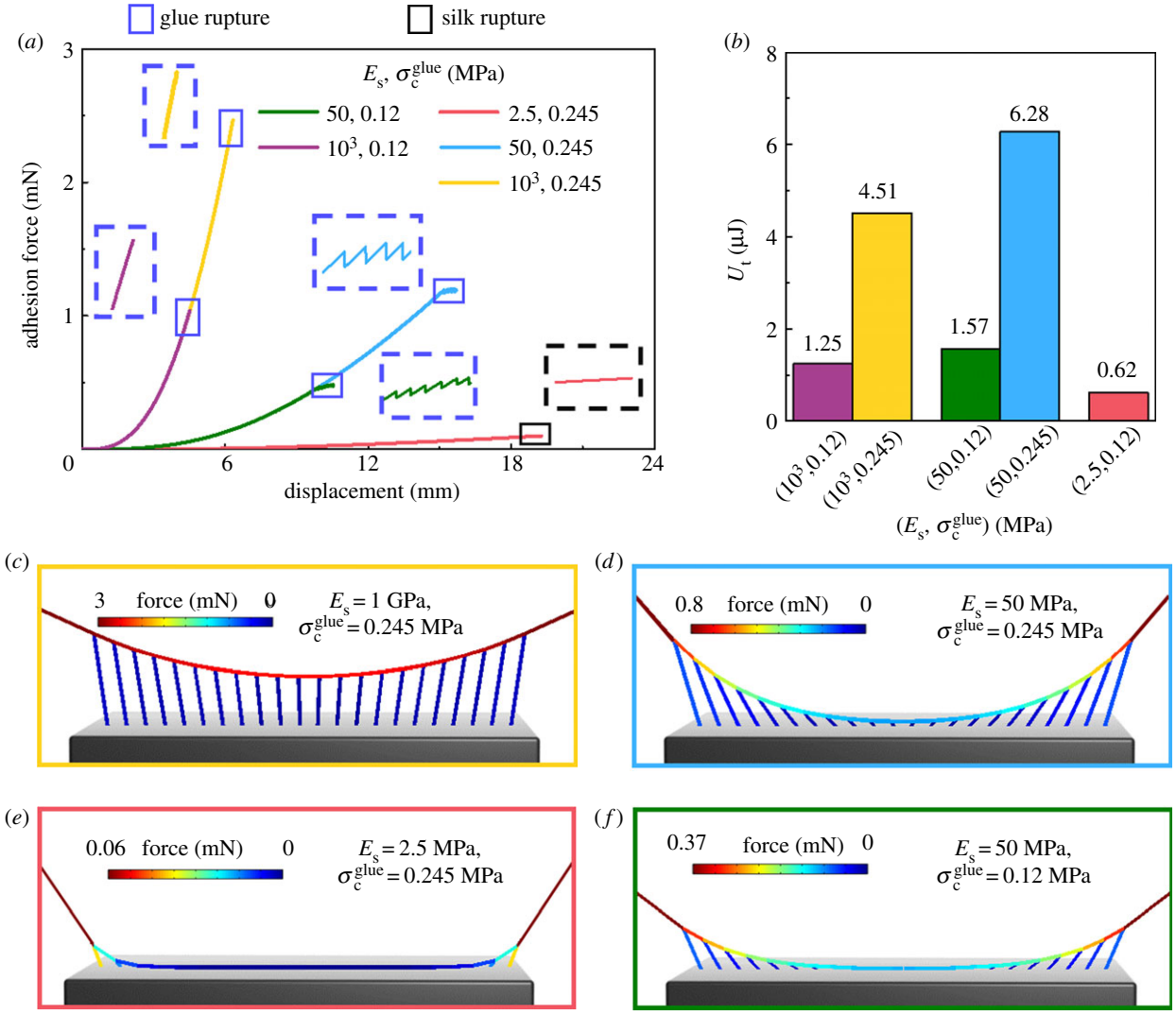

Figure 3. Synergetic effect of silk fibre elasticity E_s and glue droplet strength σ_c^{glue}. (*a*) Force–displacement curves of a capture silk thread peeled from a substrate under different values of E_s and σ_c^{glue}. The insets give the magnified curves at the late stage of peeling before full detachment. (*b*) Comparison of energy absorptions during peel-off test for systems with different values of E_s and σ_c^{glue}. (*c–f*) The configurations of silk–substrate systems right before the first droplet breakage or silk thread rupture for different systems. (Online version in colour.)

width w, are kept the same as those measured in our experiments. The force–displacement curves for different combinations of the parameters are calculated and shown in figure 3*a*, where the insets give the zoom-in view of the curves just before full detachment. The corresponding energy absorptions U_t for the force–displacement curves are shown in figure 3*b*. Figure 3*c–f* show the configurations in the critical state at which the first detachment of glue droplets or silk thread rupture occurs.

It can be seen from figure 3*a* that the force–displacement curve for stiffer silk ($E_s = 1$ GPa and $\sigma_c^{glue} = 0.245$ MPa, yellow curve) has a larger maximum adhesion force F_{max} but a smaller detachment displacement d_{max} compared to those of the real capture silk (blue curve). Because of the short detachment displacement, the stiffer silk ($E_s = 1$ GPa and $\sigma_c^{glue} = 0.245$ MPa) can only dissipate 4.51 μJ of energy during the peeling process, which is 28.2% lower than the real capture silk (6.28 μJ), as in figure 3*b*. Another reason for this relatively low energy absorption is that all glue droplets are detached from the substrate almost simultaneously for the stiff silk and only stage I contributes to the energy absorption. Therefore, an overly stiff capture silk would noticeably impair the energy absorption capacity of the orb web.

By contrast, if the silk has a lower elastic modulus than the real value (e.g. $E_s = 2.5$ MPa), the force–displacement curve would have a larger detachment displacement d_{max} but a significantly lower maximum adhesion force F_{max}. Because of the reduction in adhesion force, the compliant silk can absorb only a small amount of energy approximately 0.62 μJ. Figure 3*e* shows the force distribution in this case, indicating that there exist high force concentrations in the glue droplets near the contact edge and the external load cannot be uniformly distributed over the contact zone. Because of its compliance, the silk now has a much larger strain as the external load increases. The overly compliant silk can even break prior to the detachment of the glue droplets during the peeling process. This again severely limits the energy absorption of the system and the spider web will be damaged after peeling. The above analysis suggests that the capture silk should have an optimal stiffness that can not only endow it with a superior energy absorption ability but also guarantee its structural integrity during prey capture.

We also examine the influence of glue adhesion strength σ_c^{glue} on the peeling process. The force–displacement curves in figure 3*a* show that for a fixed elastic modulus, both d_{max} and F_{max} increase with increasing σ_c^{glue}. It can be found that

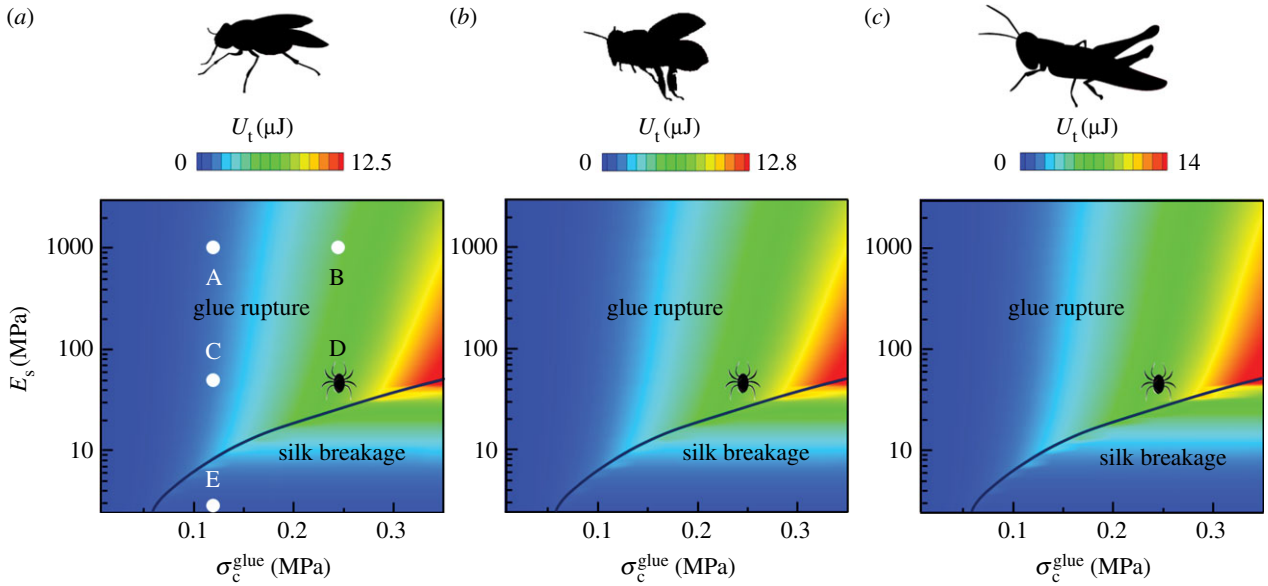

Figure 4. Optimal combination of silk stiffness and glue strength that yields highest energy absorption in capturing different prey. The energy absorption capabilities during the peeling process are given with respective to silk's elastic modulus E_s and glue's tensile strength σ_c^{glue} when the adhesion size w is similar to (*a*) a fly, (*b*) a honeybee and (*c*) a locust. The solid black curves represent the optimal value of E_s that maximizes the energy absorption U_t under a given σ_c^{glue}. The position of the spider drawn in each figure corresponds to the mechanical properties of the real capture silk thread and the glue droplets. The parameters at points A–E in (*a*) are the same as those in the force–displacement curves in figure 3*a*. (Online version in colour.)

the glue strength σ_c^{glue} has little influence on the geometric feature and force distribution inside the silk–substrate system during stage I (figure 3*d*,*f*), as their force–displacement curves are similar to each other in the beginning regime.

3.3. Energy absorption capability to capture prey items of different sizes

In this section, we examine the energy absorption capability of the capture silk when adhered to objects with different widths. The energy comes from the work done by the struggling prey item, which includes two parts, i.e. the elastic strain energy in the threads during deformation and the fracture energy of the glue droplets when the prey item is removed. In the simulations, fly, honeybee and locust are chosen as three representative insects of prey and their abdomen widths are taken as the size of the initial contact zone width, w (given in electronic supplementary material).

To find the optimal combination of the mechanical properties of silk and glue for optimal capture performance, the total energy absorption during the peeling process, U_t, is calculated as a function of the silk modulus E_s and glue strength σ_c^{glue}. For three typical sizes of adhesion, the energy absorptions U_t are given in figure 4 as functions of E_s and σ_c^{glue}. It can be seen from figure 4 that for each set of the glue strength σ_c^{glue} and a specified contact zone width w, there is an optimal value of E_s that can yield the maximum energy absorption U_t. For the three kinds of prey (fly, honeybee and locust), the optimal combinations of (E_s, σ_c^{glue}) are given by the black solid curves in figure 4*a*–*c*, respectively. In each figure, the combination of the real capture silk thread is indicated by a marker with the spider silhouette (black in colour) in (E_s, σ_c^{glue}) space. The computational results indicate that the mechanical properties of the real capture silk thread are close to the optimal (E_s, σ_c^{glue}) curve in all three cases. This suggests that the capture silk thread has evolved with an optimized energy absorption ability for a variety of prey with different body sizes. Artificially increasing or lowering the elastic modulus E_s than their actual values would result in a decrease in U_t. For example, we compare the energy absorptions of the five different combinations of silk's elastic modulus E_s and glue's strength σ_c^{glue} as calculated in figure 3*a* and mark them as A–E in figure 4*a*. It is seen that the energy absorption U_t of the real silk is the highest among all five combinations.

Even though the stiffer silk and the stronger glue droplets would result in higher energy absorption (red part in figure 4), some trade-offs may limit the real energy absorption. For example, it is costly for the spider to produce stiffer silk threads (e.g., higher spinning speeds [42]). Furthermore, glue strength is limited by both the strength of the glue and the adhesion strength of the glue–substrate interface [29].

3.4. Scaling law for optimal combination of silk stiffness, strength and glue strength

In this section, we derive a scaling law to determine the optimal value of silk's elastic modulus E_s that maximizes the total energy absorption U_t under a specified glue strength σ_c^{glue}. It is noticed that the optimal combination of (E_s, σ_c^{glue}) corresponds to the case where the silk thread breakage and glue detachment occur simultaneously. The total energy absorption U_t before system failure contains the elastic strain energies stored in the silk (U_s) and glue droplets (U_g). Because the deformation of the silk thread is typically much larger than that of the glue droplets during peeling, by neglecting U_g and the energy difference of silk thread between suspended segment and contact zone, we can estimate the total energy absorption U_t as

$$U_t = E_s A_0 L_0 \varepsilon_{rupture}^2, \tag{3.1}$$

where $\varepsilon_{rupture}$ is the critical tensile strain in the silk thread when system failure occurs (i.e. either the silk thread breaks

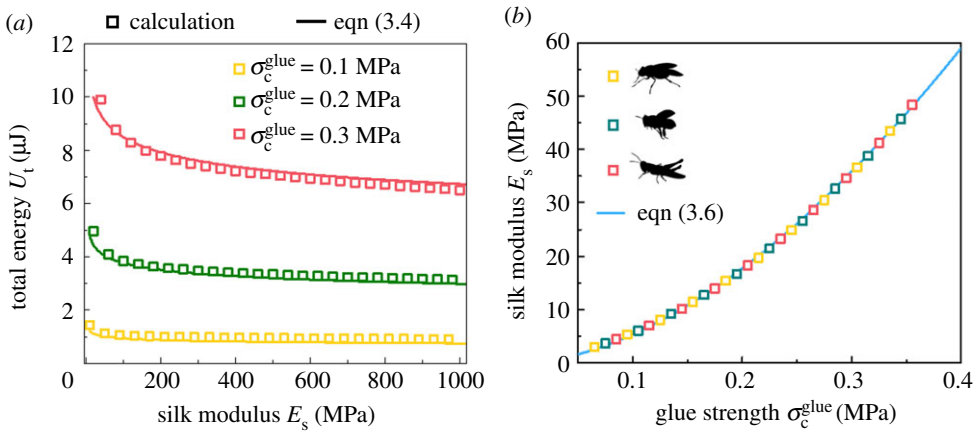

Figure 5. Scaling law for the optimal combination of silk stiffness and glue strength. (*a*) Variations in the total energy absorption U_t with respect to the elastic modulus E_s of silk and the tensile strength σ_c^{glue} of glue. (*b*) Comparison between the scaling law in equation (3.6) and numerical simulations for the optimal $E_s - \sigma_c^{glue}$ curve for prey of different contact zone width w. (Online version in colour.)

or the final detachment occurs). At silk thread breakage, $\varepsilon_{rupture}$ is equal to the breaking strain of the silk, ε_c^{silk} and equation (3.1) becomes

$$U_t = E_s A_0 L_0 (\varepsilon_c^{silk})^2. \tag{3.2}$$

At glue droplet detachment, through a dimensional analysis and theoretical analysis, $\varepsilon_{rupture}$ is related to the critical tensile force of glue, F_c^{glue}, by

$$\varepsilon_{rupture} = k\left(\frac{F_c^{glue}}{E_s A_0}\right)\left(\frac{K_s}{K_g}\right)^m, \tag{3.3}$$

where k and m are two dimensionless parameters. From equations (3.1) and (3.3), the total energy absorption U_t can be expressed as

$$U_t = \frac{(kF_c^{glue})^2}{K_s}\left(\frac{K_s}{K_g}\right)^{2m}. \tag{3.4}$$

Figure 5*a* shows the relationship between U_t and silk's elastic modulus E_s (i.e. K_s) from numerical calculation and equation (3.4) with $k = 8.04$ and $m = 0.45$.

The above relations allow us to determine the optimal $E_s - \sigma_c^{glue}$ curve. Under each optimal combination of (E_s, σ_c^{glue}), one has $\varepsilon_{rupture} = \varepsilon_c^{silk}$. Thus, the optimal $E_s - \sigma_c^{glue}$ relation can be derived from equation (3.3) as

$$E_s = k\left(\frac{A_g}{A_0}\right)\left(\frac{K_s}{K_g}\right)^m \frac{\sigma_c^{glue}}{\varepsilon_c^{silk}}. \tag{3.5}$$

Letting $K_s = E_s A_0 / L_0$, from $K_s = 2E_s A_0/(2L_0 - w)$ by ignoring the contact zone width w, equation (3.5) is rewritten as

$$E_s^{1-m} = k\left(\frac{A_g}{A_0}\right)\left(\frac{A_0}{L_0}\right)^m \frac{\sigma_c^{glue}}{\varepsilon_c^{silk} K_g^m}. \tag{3.6}$$

The scaling law in equation (3.6) is shown in good agreement with the numerical simulation results in figure 5*b*. It can be seen from figure 5*b* that the optimal $E_s - \sigma_c^{glue}$ curve is almost independent of the contact zone width w, indicating that the mechanical properties in the silk–glue system are optimized for prey with a wide range of sizes. However, we need to emphasize that the optimal relation between silk stiffness and glue adhesion strength in the simplified scaling law does not depend on w yet the absolution value of adhesion energy still relies on w.

Finally, it is emphasized that the mechanical properties of the real capture silk, though close to the optimal $E_s - \sigma_c^{glue}$ curves, are located in the regime of glue droplet rupture for all three cases (fly, honeybee and locust) considered in figure 4 [27]. This seemingly conservative feature can be beneficial from the point of view of structural integrity of the spider web. This is consistent with our experimental observation that no silk breakage was observed in any of the peeling experiments.

4. Conclusion

We have studied the peeling-induced detachment between a spider capture silk thread and a solid substrate via both experiments and theoretical analysis. Particular attention has been given to the synergistic effects of the stiffness of the capture silk and the stickiness of its adhesive glue droplets. In contrast to the common view that silk adhesion is determined primarily by the glue stickiness, we have shown that the stiffness of the silk can significantly affect the energy dissipation during peeling. For a given adhesion strength of the glue droplets, there exists an optimal elastic modulus of the silk for the maximum energy absorption during peeling. A scaling law based on dimensional analysis reveals the quantitative correlation between the optimal silk stiffness and glue strength. Our experiments and analysis suggest that the mechanical properties of capture silk are optimal, ensuring an outstanding energy absorption capacity and a self-protecting mechanism for structural integrity. The present work provides physical insights into the working principle of spider adhesion and may be used as a guideline for the biomimetic design of spider-inspired adhesion and capture devices.

Data accessibility. Electronic supplementary material supporting this article is available through download. This includes electronic supplementary material, video S1, figures S1 and S2.

Authors' contributions. Q.L., H.-P.Z., X.-Q.F. and H.G. conceived and designed the research. Y.G., Z.C. and H.-Y.G. carried out the experiments. Y.G., H.-Y.G., X.-Q.F. and W.F. established the model and ran the simulations. All authors contributed to writing the manuscript.

Competing interests. We declare we have no competing interests.

Funding. Support from the National Natural Science Foundation of China (Grant Nos. 11432008, 11372162 and 11602294) are acknowledged.

Acknowledgements. The authors thank Y. Zhao, Z. L. Zhao, J. Zhang and S. S. Qiao for their help with the experiments.

References

1. Peppas NA, Langer R. 1994 New challenges in biomaterials. *Science* **263**, 1715–1720. (doi:10.1126/science.8134835)
2. Maboudian R. 1998 Adhesion and friction issues associated with reliable operation of MEMS. *MRS Bull.* **23**, 47–51. (doi:10.1557/S0883769400030633)
3. Kim S, Laschi C, Trimmer B. 2013 Soft robotics: a bioinspired evolution in robotics. *Trends Biotechnol.* **31**, 287–294. (doi:10.1016/j.tibtech.2013.03.002)
4. Creton C, Papon E. 2003 Materials science of adhesives: how to bond things together. *MRS Bull.* **28**, 419–423. (doi:10.1557/mrs2003.121)
5. Tian Y, Pesika N, Zeng H, Rosenberg K, Zhao B, Mcguiggan P, Autumn K, Israelachvili J. 2006 Adhesion and friction in gecko toe attachment and detachment. *Proc. Natl Acad. Sci. USA* **103**, 19 320–19 325. (doi:10.1073/pnas.0608841103)
6. Kleinteich T, Gorb SN. 2014 Tongue adhesion in the horned frog *Ceratophrys* sp. *Sci. Rep.* **4**, 1314. (doi:10.1038/srep05225)
7. Lee H, Messersmith PB. 2006 Single-molecule mechanics of mussel adhesion. *Proc. Natl Acad. Sci. USA* **103**, 12 999–13 003. (doi:10.1073/pnas.0605552103)
8. Ogaki R, Alexander M, Kingshott P. 2010 Chemical patterning in biointerface science. *Mater. Today* **13**, 22–35. (doi:10.1016/S1369-7021(10)70057-2)
9. Guo HY, Li Q, Zhao HP, Zhou K, Feng XQ. 2015 Functional map of biological and biomimetic materials with hierarchical surface structures. *RSC Adv.* **5**, 66 901–66 926. (doi:10.1039/C5RA09490A)
10. Tarakanova A, Buehler MJ. 2012 The role of capture spiral silk properties in the diversification of orb webs. *J. R. Soc. Interface* **9**, 3240–3248. (doi:10.1098/rsif.2012.0473)
11. University of Oxford. 2014 How electricity helps spider webs snatch prey and pollutants. *ScienceDaily*, 8 December 2013.
12. Foelix RF. 2011 *Biology of spiders*, 3rd edn. Oxford, UK: Oxford University Press.
13. Omenetto FG, Kaplan DL. 2012 Spider webs: damage control. *Nat. Mater.* **11**, 273–274. (doi:10.1038/nmat3291)
14. Sensenig AT, Lorentz KA, Kelly SP, Blackledge TA. 2012 Spider orb webs rely on radial threads to absorb prey kinetic energy. *J. R. Soc. Interface* **9**, 1880–1891. (doi:10.1098/rsif.2011.0851)
15. Blackledge TA, Scharff N, Coddington JA, Szuts T, Wenzel JW, Hayashi CY, Agnarsson I. 2009 Reconstructing web evolution and spider diversification in the molecular era. *Proc. Natl Acad. Sci. USA* **106**, 5229–5234. (doi:10.1073/pnas.0901377106)
16. Nyffeler M, Knornschild M. 2013 Bat predation by spiders. *PLoS ONE* **8**, e58120. (doi:10.1371/journal.pone.0058120)
17. Cox JA, NeSmith CC. 2007 Acadian flycatcher caught in the web of a golden silk orb-weaver. *Florida Field Naturalist* **35**, 46–48.
18. Vollrath F, Fairbrother WJ, Williams RJP, Tillinghast EK, Bernstein DT, Gallagher KS, Townley MA. 1990 Compounds in the droplets of the orb spider's viscid spiral. *Nature* **345**, 526–528. (doi:10.1038/345526a0)
19. Omenetto FG, Kaplan DL. 2010 New opportunities for an ancient material. *Science* **329**, 528–531. (doi:10.1126/science.1188936)
20. Aoyanagi Y, Okumura K. 2010 Simple model for the mechanics of spider webs. *Phys. Rev. Lett.* **104**, 038102. (doi:10.1103/PhysRevLett.104.038102)
21. Torres FG, Troncoso OP, Cavalie F. 2014 Physical characterization of the liquid adhesive from orb-weaving spiders. *Mater. Sci. Eng. C* **34**, 341–344. (doi:10.1016/j.msec.2013.09.030)
22. Sahni V, Blackledge TA, Dhinojwala A. 2011 A review on spider silk adhesion. *J. Adhes.* **87**, 595–614. (doi:10.1080/00218464.2011.583588)
23. Sahni V, Blackledge TA, Dhinojwala A. 2010 Viscoelastic solids explain spider web stickiness. *Nat. Commun.* **1**, 19. (doi:10.1038/ncomms1019)
24. Opell BD, Hendricks ML. 2010 The role of granules within viscous capture threads of orb-weaving spiders. *J. Exp. Biol.* **213**, 339–346. (doi:10.1242/jeb.036947)
25. Opell BD, Hendricks ML. 2009 The adhesive delivery system of viscous capture threads spun by orb-weaving spiders. *J. Exp. Biol.* **212**, 3026–3034. (doi:10.1242/jeb.030064)
26. Opell BD, Hendricks ML. 2007 Adhesive recruitment by the viscous capture threads of araneoid orb-weaving spiders. *J. Exp. Biol.* **210**, 553–560. (doi:10.1242/jeb.02682)
27. Agnarsson I, Blackledge TA. 2009 Can a spider web be too sticky? Tensile mechanics constrains the evolution of capture spiral stickiness in orb-weaving spiders. *J. Zool.* **278**, 134–140. (doi:10.1111/j.1469-7998.2009.00558.x)
28. Amarpuri G, Zhang C, Diaz C, Opell BD, Blackledge TA, Dhinojwala A. 2015 Spiders tune glue viscosity to maximize adhesion. *ACS Nano* **9**, 11 472–11 478. (doi:10.1021/acsnano.5b05658)
29. Amarpuri G, Zhang C, Blackledge TA, Dhinojwala A. 2017 Adhesion modulation using glue droplet spreading in spider capture silk. *J. R. Soc. Interface* **14**, 20160228. (doi:10.1098/rsif.2017.0228)
30. Opell BD, Karinshak SE, Sigler MA. 2011 Humidity affects the extensibility of an orb-weaving spider's viscous thread droplets. *J. Exp. Biol.* **214**, 2988–2993. (doi:10.1242/jeb.055996)
31. Opell BD, Karinshak SE, Sigler MA. 2013 Environmental response and adaptation of glycoprotein glue within the droplets of viscous prey capture threads from araneoid spider orb-webs. *J. Exp. Biol.* **216**, 3023–3034. (doi:10.1242/jeb.084822)
32. Opell BD, Buccella KE, Godwin MK, Rivas MX, Hendricks ML. 2017 Humidity-mediated changes in an orb spider's glycoprotein adhesive impact prey retention time. *J. Exp. Biol.* **220**, 1313–1321. (doi:10.1242/jeb.148080)
33. Stellwagen SD, Opell BD, Short KG. 2014 Temperature mediates the effect of humidity on the viscoelasticity of glycoprotein glue within the droplets of an orb-weaving spider's prey capture threads. *J. Exp. Biol.* **217**, 1563–1569. (doi:10.1242/jeb.097816)
34. Stellwagen SD, Opell BD, Clouse ME. 2015 The impact of UVB radiation on the glycoprotein glue of orb-weaving spider capture thread. *J. Exp. Biol.* **218**, 2675–2684. (doi:10.1242/jeb.123067)
35. Opell BD, Schwend HS, Vito ST. 2011 Constraints on the adhesion of viscous threads spun by orb-weaving spiders: the tensile strength of glycoprotein glue exceeds its adhesion. *J. Exp. Biol.* **214**, 2237–2241. (doi:10.1242/jeb.055707)
36. Blamires SJ, Martens PJ, Kasumovic MM. 2018 Fitness consequences of plasticity in an extended phenotype. *J. Exp. Biol.* **221**, jeb.167288. (doi:10.1242/jeb.167288)
37. Sahni V, Miyoshi T, Chen K, Jain D, Blamires SJ, Blackledge TA, Dhinojwala A. 2014 Direct solvation of glycoproteins by salts in spider silk glues enhances adhesion and helps to explain the evolution of modern spider orb webs. *Biomacromolecules* **15**, 1225–1232. (doi:10.1021/bm401800y)
38. Liao CP, Blamires SJ, Hendricks ML, Opell BD. 2015 A re-evaluation of the formula to estimate the volume of orb web glue droplets. *J. Arachnology* **43**, 97–100. (doi: 10.1636/M14-50.1)
39. Elettro H, Neukirch S, Vollrath F, Antkowiak A. 2016 In-drop capillary spooling of spider capture thread inspires hybrid fibers with mixed solid–liquid mechanical properties. *Proc. Natl Acad. Sci. USA* **113**, 6143–6147. (doi:10.1073/pnas.1602451113)
40. Gosline JM, Guerette PA, Ortlepp CS, Savage KN. 1999 The mechanical design of spider silks: from fibroin sequence to mechanical function. *J. Exp. Biol.* **202**, 3295–3303.
41. Blackledge TA, Hayashi CY. 2006 Silken toolkits: biomechanics of silk fibers spun by the orb web spider *Argiope argentata* (Fabricius 1775). *J. Exp. Biol.* **209**, 2452–2461. (doi:10.1242/jeb.02275)
42. Liu Y, Shao Z, Vollrath F. 2005 Relationships between supercontraction and mechanical properties of spider silk. *Nat. Mater.* **4**, 901–905. (doi:10.1038/nmat1534)